An OSMR-CLIC1 cross talk drives key oncogenic pathways in glioblastoma

Amir Hossein Mansourabadi[1,2,3,*], Kamaldeep Randhawa[1,2,3,*], Jamie Snider[4,*], Dianbo Qu[1,2,3], Francesca Cianci[5] Max Kotlyar[6], Guido Rey[5], Laura Raco[1,2,3,7], Dylan Burger[1,8], Janusz Rak[9], Vahab Soleimani[10], Igor Jurisica[6,11,12], Michele Mazzanti[5], Igor Stagljar[4,13,14,15,¶], Arezu Jahani-Asl[1,2,3,7,16,17, ¶]

[1]Department of Cellular and Molecular Medicine, Faculty of Medicine, University of Ottawa, 451 Smyth Road, K1H 8M5, Ottawa, Canada
[2]University of Ottawa Brain and Mind Research Institute, 451 Smyth Road, K1H 8M5, Ottawa, Canada
[3]Ottawa Institute of Systems Biology, 451 Smyth Road K1H 8M5, Ottawa, Canada
[4]Donnelly Centre, University of Toronto, Ontario, Canada
[5]Laboratory of Cellular and Molecular Physiology, Department of Biosciences, University of Milano, Via Celoria 26, I-20133, Milano, Italy
[6]Osteoarthritis Research Program, Division of Orthopedic Surgery, Schroeder Arthritis Institute, and Data Science Discovery Centre for Chronic Diseases, Krembil Research Institute, University Health Network, 60 Leonard Avenue, 5KD-407, Toronto, Ontario, Canada M5T 0S8
[7]Division of Clinical and Translational Research, McGill University, 1001 Decarie Boulevard Montreal (Quebec) H4A 3J1
[8]Kidney Research Centre, Inflammation & Chronic Disease Program, Ottawa Hospital Research Institute, Ottawa, ON, K1H 8L6, Canada.
[9]Department of Pediatrics, Faculty of Medicine and Health Sciences, McGill University
[10]Department of Biochemistry, Microbiology and Immunology, Faculty of Medicine, University of Ottawa, 451 Smyth Road K1H 8M5, Ottawa, Canada
[11]Departments of Medical Biophysics and Computer Science, and Faculty of Dentistry, University of Toronto
[12]Institute of Neuroimmunology, Slovak Academy of Sciences, Bratislava, Slovakia
[13]Mediterranean Institute for Life Sciences, Meštrovićevo Šetalište 45, HR-21000 Split, Croatia
[14]Department of Biochemistry, University of Toronto, Ontario, Canada
[15]Department of Molecular Genetics, University of Toronto, Ontario, Canada
[16]Regenerative Medicine Program and Cancer Therapeutics Program, Ottawa Hospital Research Institute, Ottawa, ON, K1H 8L6, Canada.
[17]Gerald Bronfman Department of Oncology, McGill University, 5100 de Maisonneuve Blvd. West, Montréal, QC, H4A 3T2, Canada.
[*]Authors contributed equally
[¶]Correspondence: igor.stagljar@utoronto.ca, arezu.jahani@uottawa.ca

ABSTRACT

The cytokine receptor Oncostatin M receptor (OSMR) plays diverse and important roles in several human malignancies, including brain, breast, and pancreatic cancer[1-4]. In glioblastoma (GB), OSMR orchestrates a feedforward loop with the oncogenic EGFRvIII and STAT3, promoting tumor progression[4]. Beyond EGFRvIII, OSMR promotes cancer stem cells via upregulation of mitochondrial oxidative phosphorylation (OXPHOS), and contributes to therapy resistance[5]. However, the molecular mechanisms governing the multifaceted roles of OSMR remain poorly understood. Here, we systematically mapped the OSMR interactome with and without EGFRvIII expression using Mammalian Membrane Two-Hybrid High-Throughput Screening (MaMTH-HTS). This unbiased approach enabled us to identify OSMR-specific and OSMR/EGFRvIII-specific binding proteins, revealing context-dependent OSMR functions. Among a subset of common interactors, we uncovered chloride intracellular channel 1 (CLIC1) as a critical regulator of both OSMR-STAT3 signaling and the OSMR/EGFRvIII oncogenic complex in GB. We demonstrate that CLIC1 physically associates with both OSMR and EGFRvIII and plays a key role in EGFRvIII packaging into extracellular vesicles (EVs). Genetic deletion of CLIC1 disrupts the OSMR/EGFRvIII interaction, impairs STAT3 activation, reduces EGFRvIII EV content, and inhibits GB growth. Using whole-cell patch-clamp recordings and a monoclonal antibody that selectively targets plasma membrane CLIC1 (tmCLIC1omab), we show that the membrane configuration of the CLIC1 is essential for sustaining EGFRvIII/STAT3 signaling. We establish a distinct pharmacologically and biophysically regulated tmCLIC-mediated current. Furthermore, we show that OSMR is required for maintaining CLIC1-mediated ionic homeostasis at the plasma membrane, revealing a bidirectional cross-talk between OSMR and CLIC1 that contributes to GB progression.

Main

Oncostatin M (OSM) receptor (OSMR) is a type 1 cytokine receptor with its expression highly elevated in different malignancies including glioma, melanoma, sarcoma, and breast cancer. OSMR plays a crucial role in mediating signal transduction initiated by the ligand OSM secreted by immune cells in the tumour microenvironment[1,6]. The OSM-OSMR interaction results in signal transduction via STAT3 as well as the activation of key oncogenic pathways including the phosphoinositide 3-kinase (PI3K)–AKT pathway, c-Jun N-terminal

kinases/mitogen-activated protein kinase (JNK/MAPK), and RAS/MAPK pathways[7-9]. GB exhibits different molecular subtypes each possessing distinct transcriptional and phenotypic characteristics. Each subtype exhibits intrinsic genetic and molecular elements that aid in defining the subtype; however, these states exist on a continuum rather than as separate entities[10-12]. The most common genetic alteration in GB is the amplification or activating mutation of the epidermal growth factor receptor (EGFR), with EGFR variant III (EGFRvIII) as the most common active mutant presenting in more than 30% of GB patients. EGFRvIII has been initially assigned to the aggressive classical subtype of GB. The mesenchymal subtype has been described as one of the most malignant and chemo resistant brain tumours. The aggressive nature of classical and mesenchymal subtypes can be attributed in part to the activity of the transcription factors including signal transducer and activator of transcription 3 (STAT3). These elements endow the cells with the ability to enter an epithelial-to-mesenchymal (EMT)-like states, maintain stemness, and metastasize[12]. Several studies highlight the importance of understanding the molecular heterogeneity within and between these subtypes[13,14].

Recent studies have revealed that OSMR is a key player in the regulation of classical and mesenchymal GB subtypes. OSMR functions as a co-receptor for EGFRvIII, inducing a positive feedback loop with STAT3. It also plays a crucial role in upregulating mitochondrial respiration, and conferring resistance to ionizing radiation (IR) therapy[4,5]. Additionally, OSMR is a key regulator of brain tumour stem cell (BTSC) self-renewal[5] and the immune microenvironment[15], suggesting that its function is highly context-dependent and influenced by its interaction network. However, the precise molecular mechanisms through which OSMR mediates its effects and the identity of its key interacting partners remain unclear**.**

To address this, we employed Mammalian Membrane Two-Hybrid High-Throughput Screening (MaMTH-HTS), a technology uniquely suited to identifying interacting partners of integral membrane proteins. Our screening revealed that OSMR physically and functionally interacts with transmembrane chloride intracellular channel 1 (tmCLIC1)**,** positioning it as a central player in both OSM/OSMR cytokine signaling and the OSMR/EGFRvIII co-receptor complex. We demonstrate that the genetic deletion of tmCLIC1, and pharmacological inhibition of tmCLIC1 impairs BTSCs, and oncogenic EGFRvIII/STAT3 signaling. Furthermore, our data show that OSMR is essential for the plasma membrane localization and function of CLIC1,

highlighting a previously unrecognized crosstalk between a cytokine receptor and an ion channel in driving key oncogenic pathways in GB progression**.**

Mapping OSMR interactome via Mammalian Membrane Two-Hybrid High Throughput Screening (MaMTH-HTS)

Recent studies have led to the identification of OSMR as a key oncogenic player in GB. Genome-wide studies have revealed OSMR/EGFRvIII-common and OSMR-unique gene networks suggesting a model whereby OSMR regulates GB tumourigenesis via different mechanisms[4]. In support of this model, a mitochondrial OSMR upregulates BTSC metabolism and self-renewal, independently of EGFRvIII[5]. This raises the question of how OSMR networks with alternate molecules to confer its different functions. To address this question, we performed MaMTH-HTS in HEK293T cells expressing OSMR bait, in the presence or absence of co-expressed EGFRvIII, alongside a prey library of ~8000 open reading frames from the Human ORFeome V8.1 collection[16]. We identified 334 high-confidence candidate binding partners for OSMR (**Fig. 1, Supp. Table 1**), following rigorous analyses and exclusion of MaMTH-HTS 'frequent flyers', which was established from repeated MaMTH-HTS results of 9 'individual bait' protein control experiments, as previously described[17]. Among the identified candidates, 204 hits [including 59 plasma membrane (PM) proteins] were detected when OSMR was used as bait in the absence of EGFRvIII, and 160 candidate binding partners (including 40 PM proteins) were identified when OSMR was used as a bait in the presence of EGFRvIII (**Supp. Table 1**). Importantly, our data revealed 30 candidate binding partners of OSMR that were commonly shared by both groups, 7 of which were PM proteins. The PM proteins encompassed proteins that are integral to the membrane as well as proteins that are associated with the membrane. GO term functional analysis of protein clusters in each group revealed molecules engaged in metabolic processes and signalling as top categories underscored in each group (**Fig. 1**). Furthermore, these analyses have revealed that the GO term for immune system processes was highly enriched in OSMR-unique interactome, whereas the regulation of biogenesis processes was among top GO terms for OSMR-EGFRvIII category. This novel OSMR interactome map highlights its role in different biological processes with unique variations depending on the cell's genetic background.

Analysis of OSMR common binding partner and the involvement of CLIC1

To unravel the mechanism by which OSMR operates to promote tumour growth across different GB subtypes including tumours that naturally harbour EGFRvIII or lack of EGFRvIII, we focused on the common candidate binding partners (**Supp. Table 2**), which encompassed different classes of proteins including metabolic processes, signalling, biogenesis, development, and immune system processes. OSMR tightly regulates BTSCs[4,5], a rare population of self-renewing stem cells[18,19] that are central in conferring GB resistance to therapy and tumour recurrence[20,21]. Thus, to validate MaMTH data in the context of GB, we employed four different patient-derived BTSCs that naturally harbour EGRFvIII (BTSC73 and BTSC147) or lack of EGFRvIII (BTSC12, BTSC30) (**Supp. Table 3**). We conducted a counter-screen in which we employed siRNA (**Supp. Table 4**) targeting each of the genes encoding these proteins, followed by assessing cell viability. Our results revealed that knockdown (KD) of 12 genes demonstrated a substantial reduction in cell viability exceeding 50% across different BTSCs (**Fig. 2a-e**). These included CLEC2B, CLIC1, CREB3, CSGALNACT2, DCN, EIF2C3, GC, GPBP1, HISTH3A, IMMP2L, NAT8, and ST3GAL4. Prior to follow up investigation on select candidates, we applied additional screening criteria pertaining to the known role of these proteins in BTSCs and GB as well as their known roles in regulation of different hallmarks of cancer. These criteria led us to focus on the CLIC1, as the top candidate.

CLIC1 is highly expressed in various cancers including GB, with its expression significantly correlating with poor prognosis[22]. CLIC1 exists as a soluble cytoplasmic protein, however, under specific cellular conditions that are not favored in non-cancerous cells[23], it can translocate to the PM where it functions as an anion ion channel[24,25]. Interestingly, similar to OSMR[9], CLIC1 is also highly expressed in the mesenchymal GB subtype and enriched in the cancer stem cells[22] where it promotes proliferation[26]. We first set out to validate the results obtained from our counter screen using a pool of four siRNAs targeting CLIC1 and control non-targeting RNAi (siCTL), in different BTSCs. Following electroporation of BTSCs with CLIC1 siRNA pool, samples were analyzed by RT-qPCR and immunoblotting analyses where we showed efficient siRNA-mediated knockdown of CLIC1 by greater than 85% and a significant decline in CLIC1 protein expression level (**Fig. 2f-i, Supp. Fig. 1, Supp. Fig. 2a,b**). CLIC1 KD and control BTSCs were then subjected to PrestoBlue assay where a significant decrease in the BTSC viability was documented upon KD of CLIC1 (**Supp. Fig. 2c,d**). Furthermore, transient

knockdown of CLIC1 significantly reduced BTSC sphere size (**Supp. Fig. 2e,f**). Importantly, we conducted an extreme limiting dilution assay (ELDA)[27], and showed that knockdown of CLIC1 robustly impaired stem cell frequency (**Fig. 2j-q**).

CLIC1 interacts with both OSMR and EGFRvIII in patient derived BTSCs and is required for OSMR/EGFRvIII complex

Via conducting co-immunostaining studies using antibodies to OSMR and CLIC1, we observed that CLIC1 colocalizes with OSMR in different BTSCs (**Fig. 3a-d**). We thus asked whether CLIC1 directly interacts with OSMR endogenously. To address this question, we first conducted Proximity Ligation Assay (PLA) using OSMR and CLIC1 antibodies in different BTSCs and found the *in situ* interaction of CLIC1 with OSMR across all BTSC lines that were examined (**Fig. 3e-h**), with EGFRvIII-expressing BTSCs that harbour elevated OSMR expression, exhibiting stronger signal (**Fig. 3e,f**) compared to BTSCs lacking the EGFRvIII (**Fig. 3g,h**). In parallel, we also conducted co-immunoprecipitation (co-IP) experiments using an antibody against endogenous OSMR followed by immunoblotting with a CLIC1 antibody. We confirmed the results obtained with PLA via IP-WB in which we showed that OSMR interacts with CLIC1 endogenously in BTSCs (**Fig 3i,j**).

Next, we generated transgenic BTSCs in which we induced genetic deletion of CLIC1 using CRISPR in two different EGFRvIII-expressing BTSC73 and BTSC147 (**Fig. 3 k,l**, **Supp. Fig. 3a,b**). Similar to our findings with the transient KD experiments, monoallelic (CRISPR-a) or biallelic (CRISPR-b) genetic deletion of CLIC1 induced a robust reduction in BTSC stem cell frequency (**Fig. 3m-p**), cell viability (**Supp. Fig. 3c,d),** and sphere size (**Supp. Fig. 3e,f**). We next employed BTSCs harbouring monoallelic or biallelic deletion of CLIC1 and conducted PLA to confirm the specificity of the interaction signal. Our results showed that the PLA interaction signal of OSMR-CLIC1 was completely diminished in CLIC1 CRISPR BTSCs compared to control BTSCs (**Fig. 3q-t**).

Given that OSMR forms a co-receptor with EGFRvIII, we next asked whether CLIC1 is a component of the same complex with EGFRvIII. We conducted co-immunostaining analysis in different BTSCs and found colocalization of EGFRvIII with CLIC1 (**Fig. 4a,b**). Thus, we performed PLA experiments using antibodies to EGFRvIII and CLIC1 in control and CLIC1 CRISPR BTSCs. Our results showed *in situ* interaction of CLIC1 with EGFRvIII (**Fig. 4c,d**).

Together, we established that CLIC1 forms a complex with both OSMR and EGFRvIII in patient-derived BTSCs. Importantly, genetic deletion of CLIC1 completely abolished the interaction signal.

CLIC1 is required for OSMR/EGFRvIII interaction and STAT3 phosphorylation

OSMR is found in complex with EGFRvIII to amplify receptor tyrosine kinase (RTK) signalling[4]. Given our results that CLIC1 interacts with both OSMR and EGFRvIII, we asked whether CLIC1 is required for the OSMR/EGFRvIII complex assembly. First, we confirmed the interaction of OSMR and EGFRvIII in BTSC73 and 147 (**Fig. 3e,f**). Next, we subjected CLIC1-CRISPR and corresponding control BTSCs to PLA analysis using antibodies to OSMR and EGFRvIII. Strikingly, genetic deletion of CLIC1 significantly impaired the interaction of OSMR with EGFRvIII in each of BTSC147 and BTSC73 (**Fig. 4g-j**), confirming that CLIC1 is required for OSMR/EGFRvIII interaction. These data raised the question of whether CLIC1 is functionally required for maintaining the oncogenic OSMR or OSMR/EGFRvIII signalling. OSMR orchestrates a feedforward mechanism with EGFRvIII and STAT3 to drive GB tumourigenesis[4,28]. We thus assessed whether CLIC1 is required for the phosphorylation of STAT3 and EGFRvIII. We conducted immunoblotting experiments in CLIC1 CRISPR and control BTSC73 and BTSC147 using antibodies to STAT3-Y-705 and EGFRvIII. Strikingly, we found significant attenuation in the expression of the phospho-STAT3 and EGFRvIII in CLIC1 CRISPR BTSCs (**Fig 4k-r**). Our data suggest that CLIC1 tightly maintains the phosphorylation of EGFRvIII and STAT3.

CLIC1 drives GB tumourigenesis and maintains EGFRvIII/EGFR phosphorylation *in vivo*

Our findings on a central role of CLIC1 in regulation of OSMR/EGFRvIII interaction and EGFRvIII and STAT3 phosphorylation led us next to examine whether CLIC1 contributes to GB tumourigenesis *in vivo*. We conducted intracranial tumour assay using BTSC73, BTSC147, and corresponding CLIC1 CRISPR BTSCs lines. Our data revealed that deletion of CLIC1 significantly impaired tumourigenesis, and prolonged survival (**Fig. 5a-h**). We next subjected tumour sections obtained from the control mice as well as the smaller tumours from the CLIC1 CRISPR group to H&E staining (**Fig. 5i,j**) and immunostaining analysis using a phospho-Y1068-EGFR antibody that can detect both the phosphorylated wild type (WT) EGFR and

EGFRvIII (**Fig. 5k**). Strikingly, we found that the phosphorylation of EGFR/EGFRvIII was robustly attenuated in the mice group xenografted with CLIC1 CRISPR BTSCs. Our analysis established that the genetic deletion of CLIC1 reduces the tumor size and impairs the activation of EGFR/EGFRvIII *in vivo*.

Pharmacological inhibition of the transmembrane (tm) conformation of CLIC1 (tmCLIC1) using a monoclonal antibody impairs the phosphorylation of EGFRvIII and STAT3

Our data raised the question of how CLIC1 maintains EGFRvIII-STAT3 oncogenic pathway. CLIC1 is found as a soluble cytoplasmic protein as well as a transmembrane protein that forms an ion channel[26]. We conducted cell fractionation experiments in different BTSCs and found that CLIC1 is localized to both the membrane level and cytosol (**Supp. Fig 4**); however, the majority of CLIC1 was found in the cytoplasm. CLIC1 is shown to be packaged into extracellular vesicles (EVs) in order to target neighbouring cells[29], promoting tumour growth[29,30]. Interestingly, similar to CLIC1[22,29,31], EGFRvIII impacts various aspects of tumourigenesis not only in the cell of origin, but in the neighbouring cells, also shown to be mediated via EVs[32]. Thus, we questioned whether CLIC1 is required for the horizontal propagation of EGFRvIII to the neighboring cells. By extracting EVs from CTL BTSCs and their corresponding CLIC1 CRISPR cells, we evaluated EGFRvIII protein expression levels in the cell lysates and EV fractions. Immunoblotting analysis revealed that EGFRvIII levels were significantly reduced in CLIC-deleted EVs, suggesting a role of CLIC1 in mediating EGFRvIII packaging in EVs (**Fig. 6a-c**, **Supp. Fig. 5a,b)**. These data suggest that CLIC1 may facilitate the horizontal propagation of EGFRvIII to the neighboring cells. At the same time, it raises the question of whether tmCLIC1contributes to maintaining intracellular EGFRvIII/STAT3 signalling via altering CLIC1-mediated ionic conductance. tmCLIC1 is proposed to regulate cell cycle, pH, cell volume, and cell proliferation[33]. Given the smaller fraction of tmCLIC1 of BTSCs (**Supp. Fig. 4**), we first aimed to conduct immunostaining on non-permeabilized BTSCs using a CLIC1 antibody. Imaging analysis revealed a strong CLIC1 signal in non-permeabilized BTSCs (**Fig. 6d-f**). Thus, we set out to investigate the membrane localization and electrophysiological properties of tmCLIC1 in three distinct human BTSC lines including BTSC73, BTSC147, and BTSC30. To assess basal level tmCLIC1 levels, we used IAA94, a known blocker of CLIC1. We conducted an electrophysiological evaluation of tmCLIC1 levels at +40mV on the membranes of

CLIC1 CRISPR and control BTSCs. Our results revealed that the tmCLIC1 currents were significantly reduced in the CLIC1 CRISPR lines compared to the CTL BTSCs (**Fig. 6g**), leading to the question of whether tmCLIC1 impacts EGFRvIII/STAT3 signalling. To address this question, we generated and employed a monoclonal CLIC1 antibody (tmCLIC1omab®) that specifically inhibits tmCLIC1 and its associated ionic currents. We treated different glioma cells and BTSCs with the tmCLIC1omab or IgG control, followed by an analysis of EGFRvIII and STAT3 phosphorylation in response to the ligand OSM. The tmCLIC1 current was measured as the IAA94-sensitive current, defined as the difference between the initial current and the current after drug perfusion. Our data revealed that both the EGFR phosphorylation at tyrosine (Y) 1068 and STAT3 phosphorylation at Y705 were significantly attenuated upon inhibition of the CLIC1-mediated Cl- current by a tmCLIC1 antibody in EGFRvIII expressing BTSC 147 and 73. Importantly, tmCLIC1omab® had no impact on EGFRvIII/STAT3 signalling in BTSC30 that naturally does not harbour the EGFRvIII or elevated STAT3 expression (**Fig. 6h-m**, **Supp. Fig. 6**).

Impact of OSMR knockdown on CLIC1-Mediated Cl^- Current

We have established that OSMR physically and functionally interacts with CLIC1 to maintain EGFRvIII/STAT3 oncogenic signalling in BTSC and GB and a PM CLIC1 is engaged in regulating this process. Next, we set out to investigate whether OSMR is required for CLIC1-mediated Cl^- current. We induced KD of OSMR by using short hairpin RNA (shOSMR) in different cell lines and subjected the OSMR knockdown (KD) and control (CTL) Scrambled (SCR) cells to patch clamp experiments to evaluate whether reduced OSMR expression levels alter Cl^- currents. Cell currents were assessed both prior to (baseline) and following the addition of 100 μM of CLIC1 inhibitor, IAA94 to the bath solution (**Fig. 6n-s**). The tmCLIC1 current was measured as the IAA94-sensitive current, defined as the difference between the initial current and the current after drug perfusion. The corresponding current-voltage relationship was recorded in each group. Strikingly, our data revealed that inhibition of OSMR significantly attenuated the tmCLIC1-associated Cl^- current (**Fig. 6r-t**). Taken together, we provide data that tmCLIC1 regulates OSM/OSMR-STAT3 and OSMR/EGFRvIII oncogenic signalling and at the same time OSMR promotes tmCLIC1 function. We establish that the cooperation of OSMR with

tmCLIC1 is required to drive glioblastoma progression, and strategies to inhibit this cross-talk are a promising approach for improving glioblastoma treatment.

Discussion

In this study, we comprehensively mapped the OSMR interactome to identify its high confidence binding partners under different conditions leading to a better understanding of OSMR's multifaceted roles in GB progression. Through systematic protein-protein interaction mapping using MaMTH-HTS, followed by counter-screening and loss- and gain-of-function studies, we demonstrate that tmCLIC1 interacts with OSMR physically, independently of cellular identity, and acts as a critical regulator of diverse oncogenic pathways driven by OSMR, EGFRvIII, and STAT3. We demonstrate a bidirectional relationship for tmCLIC1-OSMR interaction, which plays a pivotal role in regulating ion conductance, thereby driving GB progression**.**

CLIC1 has been implicated in multiple malignancies, including lung cancer[34], pancreatic adenocarcinoma[35], epithelial ovarian cancer[36], and medulloblastoma[37]. It is associated with poor prognosis in GB and is abundantly expressed in cancer stem cells (CSCs)[22,38]. Previous studies have highlighted the role of tmCLIC1 in cellular proliferation and viability, with genetic deletion leading to cell swelling, mitotic defects, and reduced proliferation in medulloblastoma cells[37]. tmCLIC1 may act as a cell cycle accelerator by mediating cell volume changes. For instance, during the prophase to metaphase transition, cells undergo a significant volume decrease, reaching a minimum size at metaphase. This reduced volume is preferred by the cell and is referred to as pre-mitotic condensation[39,40]. Pre-mitotic condensation requires the efflux of Cl-, which may be mediated by tmCLIC1. tmCLIC1 has also been shown to play a prominent role in ROS production[23,41,42], and cell cycle regulation[43]. For example, IAA94-mediated inhibition of tmCLIC1 is shown to prolong the G1 phase, thereby extending the overall cell cycle duration[44]. In agreement with these findings, our data show that CLIC1 deletion suppresses BTSC self-renewal and proliferation, underscoring its role in cell cycle regulation. Given tmCLIC1's established function in maintaining redox balance[45], its knockdown likely elevates oxidative stress and disrupts redox homeostasis, thereby impairing BTSC proliferative capacity and self-renewal potential. These findings reinforce the idea that CLIC1 is a critical regulator of GB cell division and tumour aggressiveness. The interplay between ROS, tmCLIC1-generated chloride

currents, combined with evidence of tmCLIC1/OSMR interaction, highlights the need to investigate CLIC1's role in in cancer stem cells' metabolism in the context of GB. Whether similar to OSMR[5], tmCLIC1 regulates oxidative phosphorylation (OXPHOS) to maintain BTSCs and buffer ROS in the mitochondria remains to be investigated.

We further demonstrate a crucial role for CLIC1 in maintaining EGFRvIII intracellularly. This effect may also be attributed to CLIC1's role in tumour microenvironment modulation, as it is positively associated with stromal activation, epithelial-mesenchymal transition (EMT), and angiogenesis—hallmarks of GB progression[46]. Chloride channels, including CLIC1, have been implicated in innate and adaptive immune responses, particularly in phagocyte-mediated immunity. CLIC1 is required for phagosomal acidification and antigen processing, which are crucial for CD4□ T cell activation[46-48]. CLIC1-mediated regulation of macrophage-driven inflammation and ROS production may facilitate the establishment of a tumour-promoting microenvironment conducive to tumour growth and metastasis. Furthermore, CLIC1 plays a role in the innate immune system through its involvement in the activation of NLRP3 inflammasome[49]. Aberrant activity of the NLRP3 inflammasome has been implicated in the progression of several cancers including glioma[50,51]. Additionally, tmCLIC1 modulates Cl□ currents in activated microglia, particularly in response to β-amyloid protein (Aβ) stimulation[42]. Interestingly, OSMR and its ligand OSM operate in a paracrine fashion in which OSM secreted via immune cells typically binds the receptor on the tumour cells to direct oncogenic signalling. These findings suggest that OSMR-CLIC1 cross talk may influence immune surveillance, an area that requires further investigation in future studies.

It is also possible that loss of CLIC1 induces a cell shift towards a more differentiated phenotype. Previous research on cell fate dynamics supports this notion. Stockhausen et al. demonstrated that induced differentiation of BTSCs with serum leads to loss of EGFRvIII expression and decreased tumourigenic potential[52]. In another study by Gritti et al., CLIC1 expression was lost upon induction of differentiation with FBS[53]. These results suggest that both EGFRvIII and CLIC1 are important in maintaining stemness. Similarly, in another study by He et al., the chloride channel, Ano1, was found to limit the differentiation of epithelial progenitors towards cells of the secretory lineage[54]. Further studies are required to determine if the interaction of CLIC1 with EGFRvIII aids in establishing a cellular network that suppresses the BTSCs differentiation.

In this study, we provide data showing that CLIC1 regulates the horizontal transfer of EGFRvIII via EV. We observed a striking attenuation of EGFRvIII in EVs derived from CLIC1-CRISPR cells, suggesting that CLIC1 may regulate EGFRvIII packaging, thereby influencing neighboring cells. In support of this model, tmCLIC1 vesicle transfer has been implicated in glioma stem cell proliferation[29]. Furthermore, blocking of the chloride current in stem-like cells through the re-purposing of known pharmacological drugs, suggests that tmCLIC1 could be a promising target for therapy[53,55]. Similarly, tumour cells in GB are shown to impact neighboring cells via transferring EGFRvIII through EV[32]. Another study in gastric cancers revealed that the presence of CLIC1 in EVs are associated with resistance to vincristine by transferring resistance traits to neighboring cells[30]. Whether tmCLIC1 functional expression represents an adaptive mechanism enabling drug resistance in GB remains an exciting area of research to be explored.

Our findings have established that tmCLIC1 interaction with OSMR and EGFRvIII is essential for sustaining oncogenic signaling. Using a monoclonal CLIC1 antibody that can only target tmCLIC1, we establish the significance of tmCLIC1, however, the functional contribution of cytoplasmic CLIC1 and its involvement in mitochondrial and metabolic pathways remains to be investigated in GB. In conclusion, our findings establish tmCLIC1 as a central player in GB pathogenesis, orchestrating cytokine networks and enhancing the RTK signalling. Its interaction with OSMR and EGFRvIII is critical for sustaining BTSC self-renewal and GB tumourigenesis. These results highlight tmCLIC1 as a promising therapeutic target, suggesting that its inhibition, in combination with standard GB treatments, may lead to improved patient outcomes**.**

Methods and Materials

Brain tumour Stem Cell (BTSC) and generation of transgenic cell lines

The human BTSC lines 73, 147, 12, and 30 were generously provided by Dr. Samuel Weiss at the University of Calgary. They were generated in accordance with the University regulation from excess or discarded tissue collected during surgery from adult patients following informed consent from patients. BTSCs were characterised for major mutations (**Supp. Table 3**) and were cultured and maintained, as described in Supplementary methods. Transgenic CRISPR BTSCs were generated, using methods previously described[56]. To design the gRNA, Off-Spotter software, version 0.2.2 (https://cm.jefferson.edu/Off-Spotter/), was used. Two guide RNA strands (forward and reverse complement) were generated to target exons 5-9 of the CLIC1 gene.

To generate the construct, the Golden Gate Assembly Cloning strategy[57] was used in which gRNA1 and gRNA2 were cloned into pL-CRISPR.EFS.GFP (Addgene plasmid #57818), and pL-CRISPR.EFS.tRFP (Addgene plasmid, #57819), plasmids, respectively. Plasmids were sequenced (Genome Quebec), verified and electroporated [1300 volts by the AMAXA nucleofector 2b device (Lonza, #AAB1001) to deliver 3 µg of each plasmid construct (gRNA1-GFP and gRNA2-RFP) into ~2 million BTSC147 or BTSC73]. Electroporated cells were cultured in a T-75 low attachment flask at 37°C in a 5% CO_2. 48 hours after electroporation, BTSC spheres were dissociated into a single cell suspension using Accumax dissociation solution (Innovative Cell Technologies, #AM105) and subjected to Fluorescent Activated Cell Sorting (FACS) analysis using the BD FACSAriaTM Fusion (BD Biosciences) to sort for double positive GFP and RFP cells. Sorted cells were plated at a density of 1 cell/well into two 96-well plates containing 100 µl of BTSC media. Wells were monitored every two days to assess sphere formation and clonal samples were collected from multiple positive clones and were subject to genomic DNA isolation. Isolated DNA was analysed by PCR using internal primers and external primers to the gRNA-guided CAS9 cut site, designed using Primer3Plus software, version 3.3.0 (https://www.primer3plus.com/), to determine monoallelic, biallelic, or non-deletion clones. Monoallelic deletion clones in both BTSC73 and BTSC147 cell lines were determined by PCR in which the presence of one internal and one external band, suggested a possible knockdown, while a biallelic deletion was determined by a single external band. This suggested a possible knockout, on a 2% Agarose gel. Knockout or knockdown of CLIC1 was validated using RT-qPCR to determine gene expression and immunoblotting to determine protein expression. Since there we no clones identified that presented no cuts in the CLIC1 gene following incubation with the CRISPR-CAS9 construct, which could have been used as a control for CAS9, the chosen control for experiments using the CRISPR-CAS9-CLIC1 cells was that of the parental BTSC73 or BTSC147 line. The gRNA and primer sequences used in this experiment are listed in **Supp. Table 5**.

Mammalian Membrane Two-Hybrid-High Throughput Screen (MaMTH-HTS)

To identify binding partners of OSMR in the presence and absence of EGFRvIII, Mammalian Membrane Two-Hybrid (MaMTH) High Throughput Screen (HTS) technology was used as described in[17,58]. Briefly, plasmid expressing OSMR 'Bait' protein with C- terminally

fused MaMTH-HTS Bait tag (Cub-GAL4TF-P2A-tagBFP) alone or alongside plasmid expressing EGFRvIII (fused with 3xFLAG at its N-terminus) was transfected into a pooled 'Prey' library of HEK293T MaMTH-HTS reporter cell lines. The library of reporter cell lines stably expressed members of the Human ORFeome V8.1 collection (~8000 open reading frames - ORF's) fused to MaMTH-HTS Prey tag (Nub) at their N-terminus and P2A-mCherry at their C-Terminus and contained chromosomally integrated GFP reporter under the control of the GAL4 transcription factor (GAL4TF) promoter. Transfections were performed using X-tremeGene™ 9 Transfection Reagent (Roche, XTG9-RO) as specified by the manufacturer protocol. In order to induce Bait (**Supp. Fig. 7**) and Prey expression, cells were grown for 2-3 days in the presence of 0.5 µg/ml Tetracycline in the following conditions: 37°C, 5% CO_2 in DMEM containing 10% FBS, and 1% Penicillin/Streptomycin media. Cells were then harvested by trypsinization and resuspended at a concentration of 1-2 x 10^6 cell/ml in Basic Sorting Buffer (1X PBS, 5 mM EDTA, 25 mM HEPES pH 7.0, 1% BSA) and subjected to sorting by Flow Cytometry using BD FACSMelody (BD Biosciences). Cells were sequentially selected according to the following: tag-BFP fluorescence indicating 'Bait' expression, mCherry fluorescence indicating 'Prey' expression, and GFP fluorescence indicating Bait-Prey interaction. Cells were collected for analysis in DMEM containing 25% FBS and centrifuged pellets were processed in Phire Tissue Direct Dilution Buffer (ThermoFisher Scientific). Amplification of ORFs was done using Phire Tissue Direct PCR Master Mix (ThermoFisher Scientific) and products were purified using QIAquick PCR Purification Kit (Qiagen). Purified PCR products were subjected to Nextera XT library preparation and deep sequencing using the Illumina HiSeq 2500 system (150 bp single read). Sequencing data was processed and hits were identified using custom software developed using R programming language and integrated Bowtie2 alignment tool, version 2.5.2[59].

Counter-screen assay

BTSCs were transfected with siRNA using RNAiMax in a 96-well plate. Briefly, 1 pmol of siRNA and 0.1 µl of RNAiMax were each diluted in 5 µl of Opti-MEM and incubated separately for 5 minutes. The solutions were then gently combined and incubated at room temperature for 15 minutes to form transfection complexes. A total of 1,000 BTSCs per well were seeded in 80 µl of NeuroCult medium, followed by the addition of 10 µl of the siRNA-

RNAiMax complex with gentle shaking. After incubation at 37°C for 5 hours, 90 µl of NeuroCult medium was added to each well, and cells were further incubated at 37°C for 48 hours. Transfected cells were then subjected to the PrestoBlue assay to assess viability.

Generation of transient CLIC1 knockdown by short interfering RNA (siRNA)

Short Interfering RNA (siRNA) was used to generate transient knockdown (KD) in patient-derived BTSCs. BTSCs were processed into a single-cell suspension. ON TARGET-plus SMART pool human CLIC1 siRNA (Dharmacon, #L-009530-00-0005) at a concentration of 100 nM, and ON TARGET-plus non-targeting pool (Dharmacon, #D-001810-10-05), as described in supplemental methods.

Duolink Proximity Ligation Assay (PLA)

Proximity Ligation Assay was conducted following the manufacturer's protocol using the Duolink *In Situ* Red Starter Kit (Sigma, #DUO92101) as optimized by our group[60], and described in the supplemental Methods section. Briefly, PLA was conducted on BTSCs cultured on PDL-coated slides. After fixation, permeabilization, and incubation with primary antibodies targeting OSMR and CLIC1, PLA was performed using secondary antibody-conjugated oligonucleotide probes. Subsequent ligation and amplification steps allowed visualization of PLA signals under a laser scanning microscope at 40-60x magnification.

Extreme Limiting Dilution Assay (ELDA)

ELDA was performed as previously described[61], with detailed methods presented in the supplemental Methods section. Briefly, Single-cell BTSC suspensions were prepared and diluted in a growth factor-supplemented serum-free medium. Cells were plated at varying densities in 96-well plates and incubated for 7 days. After assessing sphere formation, an online software tool was used to determine the number of cells needed for a positive well and calculate the stem cell frequency (SCF).

Stereotaxic injections and bioluminescent imaging

Stereotaxic surgeries were conducted by injecting ~3 x 10^5 luciferase expressing CLIC1-CRISPR-BTSCs and control BTSCs into the right striata (0.8 mm lateral to the bregma, 1 mm

dorsal, and 2.5 mm from the pial surface). Prior to injection, BTSCs were dissociated into single-cell suspensions in serum-free, antibiotic-free medium and tested for luciferase activity using IVIS imaging system. Kaplan-Meier survival plots were generated by collecting mice at the point of reaching the end stage (major body weight loss, dehydration, hunched back, piloerection, and lethargy). Median survivals were calculated using a log-rank test with GraphPad Prism, following previously described methods[62]. Briefly, the Kaplan-Meier approach estimated the probability of survival at each time point. Before any time elapses, all mice were considered "at risk", however, no deaths occurred. Therefore, the probability of survival was input as a value of 1. Subsequently, information about the next elapsed time (day 7) included information about the how many participants experienced the event of interest (death). From this information, a survival probability was calculated using the formula: $S_{t+1} = S_t*((N_{t+1}-D_{t+1})/N_{t+1})$, where S_t represents survival probability, N_t represents number at risk, D_t represents number of events. The survival probability for each subsequent time point is calculated in a similar fashion and a stair-step survival curve is plotted. For tumour volume assessment, the mice received intraperitoneal injections of 200 µl of 15 mg/ml d-luciferin (ThermoFisher Scientific, #88292), underwent anesthesia via isoflurane inhalation, and were then subjected to weekly bioluminescence imaging using a CCD camera (IVIS, Xenogen). Subsequent collection and analysis of all bioluminescent data were performed utilizing Living Image 2.0 software (PerkinElmer, MA, USA). Briefly, after initialization of the IVIS Spectrum system and acquiring an image, the images were analyzed using "ROI tools" in the tool palette, selecting the area of interest. The IVIS imager captures pixels with specific photon intensity values, with brighter areas corresponding to higher photon detection, indicative of tumour induction.

Patch-Clamp Experiment

Patch electrodes (BB150F-8P with filaments, Science Products), with a diameter of 1.5 mm, were pulled from hard borosilicate glass on a Brown-Flaming P-87 puller (Sutter Instrument, Novato, CA) and fire polished to a tip diameter of 1-1.5 µm and an electrical resistance of 3-4 M. Cells were voltage-clamped using an Axopatch 200B amplifier (Axon Intrument) in whole-cell configuration in which After formation of giga-seal, the membrane patch is disrupted providing a direct low resistance access to cell interior, allowing recordings from ion channels of whole cell. The voltage step protocol used to isolate current/voltage

relationships consisted of 800 ms pulses from -60 mV to +60 mV (20 mV voltage steps). The holding potential was set according to the resting potential of the single cell (between -40 and -80 mV). tmCLIC1-mediated chloride currents were isolated from other ionic currents by perfusing IAA94 (100 μM) dissolved in the bath solution and by mathematical subtraction of the residual current from the control. Solution used are the following: bath solution (mM): 125 NaCl, 5.5 KCl, 24 HEPES, 1 MgCl2, 0.5 CaCl2, 5 D-Glucose, 10 NaOH; pH 7.4; Pipette solution (mM): 135 KCl, 10 Hepes, 10 NaCl; pH 7.4. Analysis was performed using Clampfit 10.2 (Molecular Devices) and OriginPro 9.1. tmCLIC1-mediated current (IAA94-sensitive current) was measured by analytical subtraction of residual ionic current after addition of inhibitor from total current (I_{TOT}) of the cell at each membrane potential tested. Current/voltage relationship were constructed plotting the averaged current density of the least 100 ms of the pulse against the corresponding membrane potential. Current density (pA/pF) results from the ratio between the ionic current (pA) and cells capacitance (pF). Statistical analyses were performed comparing the slopes (proportional to channel conductance) of the I/V curves of the different groups.

Generation of monoclonal tm-CLIC1 antibody

The tmCLIC1omab® antibody was designed (license# 11665M), targeting the N-terminal of the CLIC1 protein derived from mice. Polyclonal antibodies were obtained through a 138-day immunization protocol in which mice are immunized against a NH_2-CLIC1 synthetic peptide conjugated to OVA (ovalbumin) (NH_2-EQPQVELFVKAGSDGAKIGNC-COOH) (Glycine 0.1 M pH 3, Tris-HCl 1 M pH 8). Hybridoma cells that produced antibodies were sorted in single cells to obtain monoclonal antibodies. tmCLIC1omab® was used at a final concentration of 3.5 μg/ml.

Extracellular vesicle isolation and validation

To sequentially isolate EVs, the cell supernatant was centrifuged at 200 x g for 10 minutes, 300 x g for 10 minutes, 2,000 x g for 10 minutes, 10,000 x g for 30 minutes, and 100,000 x g for 2 hours, respectively (Optima XPN-100 ultracentrifuge, Beckman Coulter, USA). A beige/white pellet of EVs and a clear supernatant were evident post-centrifugation. After removing the supernatant and resuspending the small EV pellet in 1 ml PBS, the resulting pellet was then washed and centrifuged at 49,000 rpm for 30 minutes (Optima MAX 130K

Refrigerated Benchtop Ultracentrifuge, Beckman Coulter, USA). Isolated EVs were then visualized, measured, counted, and characterized in the range of 10-2,000 nm using a Nanoparticle Tracking Analyzer (NTA) (Particle Metrix ZetaView® Nanoparticle Tracking Analysis)[63,64]. We used size-mode analysis with ZetaView software (version 8.02.28) following calibration with polystyrene beads (105 and 500 nm). Samples were analyzed at a minimum of 9 camera positions with 2-second video length at 21°C.

Bioinformatic analysis

Novel interactions from MAMTH screen were integrated with the known interactions from the Integrated Interaction Database IID ver. 2021-05[65] and further annotated with Gene Ontology Biological Process and Cellular Component (release 2022-11-03), and a subset of pathways from the PathDIP database ver. 4[66]. Resulting network was built, annotated and analyzed using NAViGaTOR ver. 3.0.19[67]. The final figure was exported to SVG file and finalized with legends in Adobe Illustrator ver. 29.0.1.

Statistical analysis

Statistical analysis between conditions was performed using a Student *t*-test in which the mean of n=3 replicates were compared between two conditions to assess significance. Analysis was undertaken with the aid of GraphPad software 7. Data is shown as mean with standard deviation (mean ± SD). p-values less than 0.05 were considered significant and were marked with an asterisk as follows, $*P < 0.05$; $**P < 0.01$; $***P < 0.001$.

Acknowledgement

This work was supported by CIHR grants to A.J.-A and I.S., and J.R. (# 162198, #519474) and a AIRC IG grant (#24758) to M.M.; A.J.-A. is a Canada Research Chair at the University of Ottawa and is supported by Canada Foundation for Innovation (CFI) and Ontario Research Fund (ORF). I.S. is supported by CFI (#225404, #30865), ORF (RDI #34876, RE010-020), and Natural Sciences Research Council (NSERC RGPIN-2024-04314). IJ was supported in part by funding from Natural Sciences Research Council (NSERC RGPIN-2024-04314), CIHR (#519474), Canada Foundation for Innovation (CFI #225404, #30865), and Ontario Research

Fund (RDI #34876, RE010-020). The funders had no role in study design, data collection and analysis, decision to publish, or preparation of the manuscript.

References

1 Hara, T. *et al.* Interactions between cancer cells and immune cells drive transitions to mesenchymal-like states in glioblastoma. *Cancer cell* **39**, 779-792. e711 (2021).

2 Araujo, A. M. *et al.* Stromal oncostatin M cytokine promotes breast cancer progression by reprogramming the tumor microenvironment. *The Journal of clinical investigation* **132** (2022).

3 Alonso-Nocelo, M. *et al.* Macrophages direct cancer cells through a LOXL2-mediated metastatic cascade in pancreatic ductal adenocarcinoma. *Gut* **72**, 345-359 (2023).

4 Jahani-Asl, A. *et al.* Control of glioblastoma tumorigenesis by feed-forward cytokine signaling. *Nature neuroscience* **19**, 798-806 (2016).

5 Sharanek, A. *et al.* OSMR controls glioma stem cell respiration and confers resistance of glioblastoma to ionizing radiation. *Nature communications* **11**, 4116 (2020).

6 Lee, B. Y. *et al.* Heterocellular OSM-OSMR signalling reprograms fibroblasts to promote pancreatic cancer growth and metastasis. *Nature communications* **12**, 7336 (2021).

7 Dey, G. *et al.* Signaling network of Oncostatin M pathway. *Journal of Cell Communication and Signaling* **7**, 103-108 (2013).

8 Hermanns, H. M. Oncostatin M and interleukin-31: Cytokines, receptors, signal transduction and physiology. *Cytokine & growth factor reviews* **26**, 545-558 (2015).

9 Natesh, K. *et al.* Oncostatin-M differentially regulates mesenchymal and proneural signature genes in gliomas via STAT3 signaling. *Neoplasia* **17**, 225-237 (2015).

10 Zhang, P., Xia, Q., Liu, L., Li, S. & Dong, L. Current opinion on molecular characterization for GBM classification in guiding clinical diagnosis, prognosis, and therapy. *Frontiers in molecular biosciences* **7**, 562798 (2020).

11 Olar, A. & Aldape, K. D. Using the molecular classification of glioblastoma to inform personalized treatment. *The Journal of pathology* **232**, 165-177 (2014).

12 Kim, Y. *et al.* Perspective of mesenchymal transformation in glioblastoma. *Acta neuropathologica communications* **9**, 1-20 (2021).

13 Mathur, R. *et al.* Glioblastoma evolution and heterogeneity from a 3D whole-tumor perspective. *Cell* **187**, 446-463. e416 (2024).

14 Xie, T. *et al.* Pervasive structural heterogeneity rewires glioblastoma chromosomes to sustain patient-specific transcriptional programs. *Nature Communications* **15**, 3905 (2024).

15 Chen, M. *et al.* Exploring the oncostatin M (OSM) feed-forward signaling of glioblastoma via STAT3 in pan-cancer analysis. *Cancer cell international* **21**, 1-19 (2021).

16 Yang, X. *et al.* A public genome-scale lentiviral expression library of human ORFs. *Nature methods* **8**, 659-661 (2011).

17 Lim, S. H. *et al.* CFTR interactome mapping using the mammalian membrane two□hybrid high□throughput screening system. *Molecular systems biology* **18**, e10629 (2022).
18 Singh, S. & Dirks, P. B. Brain tumor stem cells: identification and concepts. *Neurosurgery Clinics* **18**, 31-38 (2007).
19 Singh, S. K. *et al.* Identification of human brain tumour initiating cells. *nature* **432**, 396-401 (2004).
20 Murat, A. *et al.* Stem cell–related "self-renewal" signature and high epidermal growth factor receptor expression associated with resistance to concomitant chemoradiotherapy in glioblastoma. *Journal of clinical oncology* **26**, 3015-3024 (2008).
21 Bao, S. *et al.* Glioma stem cells promote radioresistance by preferential activation of the DNA damage response. *nature* **444**, 756-760 (2006).
22 Setti, M. *et al.* Functional role of CLIC1 ion channel in glioblastoma-derived stem/progenitor cells. *Journal of the National Cancer Institute* **105**, 1644-1655 (2013).
23 Littler, D. R. *et al.* The intracellular chloride ion channel protein CLIC1 undergoes a redox-controlled structural transition. *Journal of Biological Chemistry* **279**, 9298-9305 (2004).
24 Ashley, R. Challenging accepted ion channel biology: p64 and the CLIC family of putative intracellular anion channel proteins. *Molecular membrane biology* **20**, 1-11 (2003).
25 Gururaja Rao, S., Patel, N. J. & Singh, H. Intracellular chloride channels: novel biomarkers in diseases. *Frontiers in physiology* **11**, 96 (2020).
26 Randhawa, K. & Jahani-Asl, A. CLIC1 regulation of cancer stem cells in glioblastoma. *Current Topics in Membranes* **92**, 99-123 (2023).
27 Hu, Y. & Smyth, G. K. ELDA: extreme limiting dilution analysis for comparing depleted and enriched populations in stem cell and other assays. *Journal of immunological methods* **347**, 70-78 (2009).
28 Villa, G. R. & Mischel, P. S. Old player, new partner: EGFRvIII and cytokine receptor signaling in glioblastoma. *Nature neuroscience* **19**, 765-767 (2016).
29 Setti, M. *et al.* Extracellular vesicle-mediated transfer of CLIC1 protein is a novel mechanism for the regulation of glioblastoma growth. *Oncotarget* **6**, 31413 (2015).
30 Zhao, K. *et al.* Exosome-mediated transfer of CLIC1 contributes to the vincristine-resistance in gastric cancer. *Molecular and cellular biochemistry* **462**, 97-105 (2019).
31 Kang, M.-K. & Kang, S.-K. Pharmacologic blockade of chloride channel synergistically enhances apoptosis of chemotherapeutic drug-resistant cancer stem cells. *Biochemical and biophysical research communications* **373**, 539-544 (2008).
32 Al-Nedawi, K. *et al.* Intercellular transfer of the oncogenic receptor EGFRvIII by microvesicles derived from tumour cells. *Nature cell biology* **10**, 619-624 (2008).
33 Peretti, M. *et al.* Chloride channels in cancer: Focus on chloride intracellular channel 1 and 4 (CLIC1 AND CLIC4) proteins in tumor development and as novel therapeutic targets. *Biochimica et Biophysica Acta (BBA)-Biomembranes* **1848**, 2523-2531 (2015).
34 Wang, W. *et al.* The expression and clinical significance of CLIC1 and HSP27 in lung adenocarcinoma. *Tumor Biology* **32**, 1199-1208 (2011).
35 Jia, N. *et al.* CLIC1 overexpression is associated with poor prognosis in pancreatic ductal adenocarcinomas. *Journal of cancer research and therapeutics* **12**, 892-896 (2016).

36 Singha, B. *et al.* CLIC1 and CLIC4 complement CA125 as a diagnostic biomarker panel for all subtypes of epithelial ovarian cancer. *Scientific reports* **8**, 14725 (2018).
37 Francisco, M. A. *et al.* Chloride intracellular channel 1 cooperates with potassium channel EAG2 to promote medulloblastoma growth. *Journal of Experimental Medicine* **217** (2020).
38 Wang, L. *et al.* Elevated expression of chloride intracellular channel 1 is correlated with poor prognosis in human gliomas. *Journal of Experimental & Clinical Cancer Research* **31**, 1-7 (2012).
39 Boucrot, E. & Kirchhausen, T. Mammalian cells change volume during mitosis. *PloS one* **3**, e1477 (2008).
40 Habela, C. W. & Sontheimer, H. Cytoplasmic volume condensation is an integral part of mitosis. *Cell cycle* **6**, 1613-1620 (2007).
41 Milton, R. H. *et al.* CLIC1 function is required for β-amyloid-induced generation of reactive oxygen species by microglia. *Journal of Neuroscience* **28**, 11488-11499 (2008).
42 Novarino, G. *et al.* Involvement of the intracellular ion channel CLIC1 in microglia-mediated β-amyloid-induced neurotoxicity. *Journal of Neuroscience* **24**, 5322-5330 (2004).
43 Valenzuela, S. M. *et al.* The nuclear chloride ion channel NCC27 is involved in regulation of the cell cycle. *The Journal of physiology* **529**, 541 (2000).
44 Peretti, M. *et al.* Mutual Influence of ROS, pH, and CLIC1 Membrane Protein in the Regulation of G1–S Phase Progression in Human Glioblastoma Stem Cells. *Molecular cancer therapeutics* **17**, 2451-2461 (2018).
45 Singh, H. & Ashley, R. H. Redox regulation of CLIC1 by cysteine residues associated with the putative channel pore. *Biophysical journal* **90**, 1628-1638 (2006).
46 Jiang, L. *et al.* Intracellular chloride channel protein CLIC1 regulates macrophage function through modulation of phagosomal acidification. *Journal of cell science* **125**, 5479-5488 (2012).
47 Westman, J. & Grinstein, S. Determinants of phagosomal pH during host-pathogen interactions. *Frontiers in cell and developmental biology* **8**, 624958 (2021).
48 Salao, K. *et al.* CLIC1 regulates dendritic cell antigen processing and presentation by modulating phagosome acidification and proteolysis. *Biology open* **5**, 620-630 (2016).
49 Domingo-Fernández, R., Coll, R. C., Kearney, J., Breit, S. & O'Neill, L. A. The intracellular chloride channel proteins CLIC1 and CLIC4 induce IL-1β transcription and activate the NLRP3 inflammasome. *Journal of Biological Chemistry* **292**, 12077-12087 (2017).
50 Kelley, N., Jeltema, D., Duan, Y. & He, Y. The NLRP3 inflammasome: an overview of mechanisms of activation and regulation. *International journal of molecular sciences* **20**, 3328 (2019).
51 Hamarsheh, S. a. & Zeiser, R. NLRP3 inflammasome activation in cancer: a double-edged sword. *Frontiers in immunology* **11**, 1444 (2020).
52 Stockhausen, M.-T., Kristoffersen, K., Stobbe, L. & Poulsen, H. S. Differentiation of glioblastoma multiforme stem-like cells leads to downregulation of EGFR and EGFRvIII and decreased tumorigenic and stem-like cell potential. *Cancer biology & therapy* **15**, 216-224 (2014).

53 Gritti, M. *et al.* Metformin repositioning as antitumoral agent: selective antiproliferative effects in human glioblastoma stem cells, via inhibition of CLIC1-mediated ion current. *Oncotarget* **5**, 11252 (2014).

54 He, M. *et al.* Chloride channels regulate differentiation and barrier functions of the mammalian airway. *Elife* **9**, e53085 (2020).

55 Barbieri, F. *et al.* Repurposed biguanide drugs in glioblastoma exert antiproliferative effects via the inhibition of intracellular chloride channel 1 activity. *Frontiers in oncology* **9**, 135 (2019).

56 Sharanek, A. *et al.* Transcriptional control of brain tumor stem cells by a carbohydrate binding protein. *Cell reports* **36** (2021).

57 Engler, C., Gruetzner, R., Kandzia, R. & Marillonnet, S. Golden gate shuffling: a one-pot DNA shuffling method based on type IIs restriction enzymes. *PloS one* **4**, e5553 (2009).

58 Petschnigg, J. *et al.* The mammalian-membrane two-hybrid assay (MaMTH) for probing membrane-protein interactions in human cells. *Nature methods* **11**, 585-592 (2014).

59 Langmead, B. & Salzberg, S. L. Fast gapped-read alignment with Bowtie 2. *Nature methods* **9**, 357-359 (2012).

60 Sharanek, A., Raco, L., Soleimani, V. D. & Jahani-Asl, A. In situ detection of protein-protein interaction by proximity ligation assay in patient derived brain tumor stem cells. *STAR protocols* **3**, 101554 (2022).

61 Rasool, D., Soleimani, V. D. & Jahani-Asl, A. in *Neuronal Cell Death: Methods and Protocols* 343-354 (Springer, 2022).

62 Luchman, H. A. *et al.* An in vivo patient-derived model of endogenous IDH1-mutant glioma. *Neuro-oncology* **14**, 184-191 (2011).

63 Myette, R. L. *et al.* Urinary podocyte-derived large extracellular vesicles are increased in paediatric idiopathic nephrotic syndrome. *Nephrology Dialysis Transplantation* **38**, 2089-2091 (2023).

64 Ruzicka, M. *et al.* Effect of hemodialysis on extracellular vesicles and circulating submicron particles. *BMC nephrology* **20**, 1-8 (2019).

65 Kotlyar, M. *et al.* IID 2021: towards context-specific protein interaction analyses by increased coverage, enhanced annotation and enrichment analysis. *Nucleic acids research* **50**, D640-D647 (2022).

66 Rahmati, S. *et al.* pathDIP 4: an extended pathway annotations and enrichment analysis resource for human, model organisms and domesticated species. *Nucleic acids research* **48**, D479-D488 (2020).

67 Brown, K. R. *et al.* NAViGaTOR: network analysis, visualization and graphing Toronto. *Bioinformatics* **25**, 3327-3329 (2009).

Figure legends

Figure 1. Mapping global binding partners of OSMR.

Using MaMTH-HTS, we mapped the OSMR interactome in the absence and presence of EGFRvIII. The interactome is represented with green edges for the novel MaMTH candidates and gray edges highlighting known interactions identified using the Integrated Interaction Database (IID). Purple edges indicate interactions both identified in MaMTH and predicted by IID. The candidate binding partners of OSMR in the absence of EGFRvIII (OSMR-specific interactors) are represented in blue. The candidate binding partners of OSMR in the presence of EGFRvIII (OSMR/EGFRvIII-specific interactors) are represented in red. The candidate binding partners of OSMR that were commonly shared by both groups are shown in the center. Go term functional annotation of the potential candidates are shown with different coloured squares.

Figure 2. Cell viability evaluation following gene silencing of candidate binding protein targets. a-e, Cell viability was assessed in four different patient-derived BTSCs (#12, #30, #73, and #147), transfected with siRNAs targeting different genes encoding candidate binding proteins. Each graph (**a-d**) is normalized to the control group transfected with a non-targeting siRNA. Data are presented as means ± SEM, n=3 biological replicates in a-d with Heatmap plot (**e**) comparing the differences across four BTSCs. The colour gradient, represented by column Z-scores, illustrates relative cell viability assessed by PrestoBlue analysis. **f-i**, Knockdown of CLIC1 was induced in BTSCs as described, and whole cell lysates were subjected to immunoblotting using a CLIC1 antibody. ACTIN was used as a loading control. **j-q**, CLIC1 knockdown and control cells were subjected to Extreme Limiting Dilution Assay n=3 biological replicates. Statistical analysis was performed using a student-t test. Data are represented as the means ± SD. $^{**}P < 0.01$.

Figure 3. CLIC1 and OSMR interact endogenously in BTSCs.

a-d, BTSCs were subjected to co-immunostaining using antibodies to CLIC1 (green) and OSMR (red). Nuclei were stained with Hoechst. Merged images depict co-localization of OSMR and CLIC1 (yellow). n=3 biological replicates. **e-h**, BTSCs 73 and 147 were subjected to proximity ligation assay (PLA) using antibodies to CLIC1 and OSMR. Each red puncta represents PLA signal. Primary antibodies were omitted for control group. Nuclei were stained with Hoechst. Scale bar, 10 µm. **i,j**, BTSCs 147 or 77 were subjected to immunoprecipitation (IP) using an OSMR antibody or IgG control and pull downs were analyzed by immunoblotting using CLIC1 antibody. **k,l**, mRNA expression of CLIC1 was confirmed by RT-qPCR in CLIC1 CRISPR BTSCs 147 and 73. Gene expression was normalized to the housekeeping gene GUSB. Data for two different clones (CRISPR-a and CRISPR-b) are shown for each BTSCs and represented as the means ± SD, n = 3. Statistical analysis was performed using a student-t test. $^{***}P < 0.001$. **m-p**, CLIC1 CRISPR and control BTSCs were subjected to ELDA and SCF was plotted. n=3 biological replicates/ Statistical analysis was preformed using a student-t test. Data are represented as the means ± SD. $^{**}P < 0.01$.

q-t, The interaction of CLIC1 and OSMR was assessed by PLA in CLIC1 CRISPR and control BTSCs as described in e-h. Nuclei were stained with Hoechst. The number of PLA puncta (red) per nucleus was quantified in CRISPR and control BTSC147 and BTSC73 (**r,t**). Data are presented as the means ± SEM. Each dot represents the number of PLA dots per nucleus. A minimum of n=3 biological replicate images was assessed for statistical analysis. Statistical analysis was performed using a student-t test. ***$P < 0.001$. Scale bar, 10 μm.

Figure 4. CLIC1 is required for the OSMR/EGFRvIII interaction and STAT3 activation.
a,b, BTSCs 73 and 147 were subjected to co-immunostaining using antibodies to CLIC1 and EGFRvIII. Representative images represent n=3 independent biological replicates. **c,d**, CLIC1 CRISPR and control BTSCs were subjected to PLA analysis using antibodies to CLIC1 and EGFRvIII. **e,f**, BTSCs 147 and 73 were subjected to PLA analysis using antibodies to OSMR and EGFRvIII (**e**) and quantification of # of PLA per nuclei are presented (**f**). **g-j**, Different CLIC1 CRISPR and BTSCs were subjected to PLA analysis using antibodies to OSMR and EGFRvIII (**g,i**). Quantification of PLA dots per nucleus per group is presented (**h,j**). Nuclei were stained with Hoechst. Scale bar, 10 μm. **k-r**, CLIC1 CRISPR and control BTSCs were subjected to immunoblotting using antibodies to P-STAT3-Y705, total STAT3, EGFRvIII, and total EGFR. ACTIN was used as loading control. Densitometric quantification of p-STAT3 to total STAT3 and (**l,n**) and EGFRvIII to total EGFR (**p,r**) are presented. Statistical analysis was performed using a student t-test. *$P < 0.05$, **$P < 0.01$, **$P < 0.001$, n=3 biological replicates.

Figure 5. Genetic deletion of CLIC1 impairs tumourigenesis, expands lifespan and suppresses EGFR/EGFRvIII activation.
a-h, CLIC1 CRISPR BTSCs (#73,) control BTSC73, CLIC1 CRISPR BTSCs (#147), and control BTSC147 were xenografted intracranially into 8 weeks old SCID male mice. IVIS imaging was conducted to evaluate tumour volume (**a,d**) and signal was quantified (**b,e**). Kaplan-Meier survival plots were graphed to evaluate animal lifespan in each group (**c,f**). Log-rank test (BTSC73) ($P < 0.0001$, $n \geq 5$ mice), BTSC#73 vs. CLIC1 CRISPR-a ($P = 0.0011$), BTSC#73 vs. CLIC1 CRISPR-b ($P = 0.001$), CLIC1 CRISPR-a vs. CLIC1 CRISPR-b ($P = 0.0014$). Log rank test for BTSC#147, ($P = 0.0078$, n=3), BTSC#147 vs. CLIC1 CRISPR-a ($P = 0.0246$), BTSC#147 vs CLIC1 CRISPR-b ($P = 0.0246$), CLIC1 CRISPR-a vs CLIC1 CRISPR-b (non-significant). Representative panels for changes in body weight following BTSC implantation are shown (**g-h**). **i-k**, Brain sections depicting tumour in control BTSC73 and CLIC1-CRISPR BTSC73 were subjected to H&E staining (**i,j**) or immunostaining with a p-EGFR-Y1068 antibody (**k**).

Figure 6. An OSMR-CLIC1 cross talk regulates key oncogenic processes
a-c, CLIC1 CRISPR and control BTSCs were subjected to extracellular vesicle (EV) isolation. EV-digested lysates and whole cell lysates were subjected to immunoblotting analysis using antibodies indicated on the blot (**a**). Quantification of EGFRvIII in EV were conducted (**b,c**),

$P < 0.01$. **d-f, Non-permeabilized BTSCs were subject to CLIC1 staining to depict plasma membrane. Nuceli are stained with Hoechst. Scale bar, 10 µm, n=3 biological replicates. **g**, Electrophysiological evaluation of transmembrane (TM)-CLIC1 was conducted at +40 mV on CLIC1 CRIPSR and control BTSCs. WT (white bar), CLIC1 +/- (monoallelic deletion, grey bar) and CLIC1 -/- (biallelic deletion, black bar). **h-m**, CLIC1 CRISPR and control BTSCs were treated with a monoclonal antibody that specifically inhibit the membrane configuration of CLIC1 (tm-CLIC1-omab) for 72 hours and were analyzed by immunoblotting using antibodies to p-STAT3, STAT3, p-EGFR and EGFR. Densitometric analysis of p-STAT3 to total STAT3 (**h,k,j,m**) and p-EGFR to total EGFR (**i,l**) in tm-CLIC1-mab treated antibodies versus control are shown, n = 3 or > 3, paired students' t test *$P < 0.05$. **$P < 0.01$. **n-q**, Representative whole cell current for cells were conducted at several voltages ranging from -60 to +60 mV with 20 mV increments in control (**n,p**) and in OSMR knockdown BTSCs (**o,q**). Currents were recorded in resting conditions (**n,o**) and after IAA94 administration (**p,q**). **r**, I/V plot for control (SCR, black circles) and after perfusion of IAA94 (empty circles), and **s**, I/V plot for shOSMR cells in CTL condition (black triangles) and after perfusion of IAA94 (empty triangles) are shown. Average current-voltage recordings at different test potentials are shown. **t**, tmCLIC1 current for four different GB cell lines were analyzed at +40 mV in shOSMR and SCR control groups. The average current for the SCR (grey) and shOSMR (black) cells are shown.

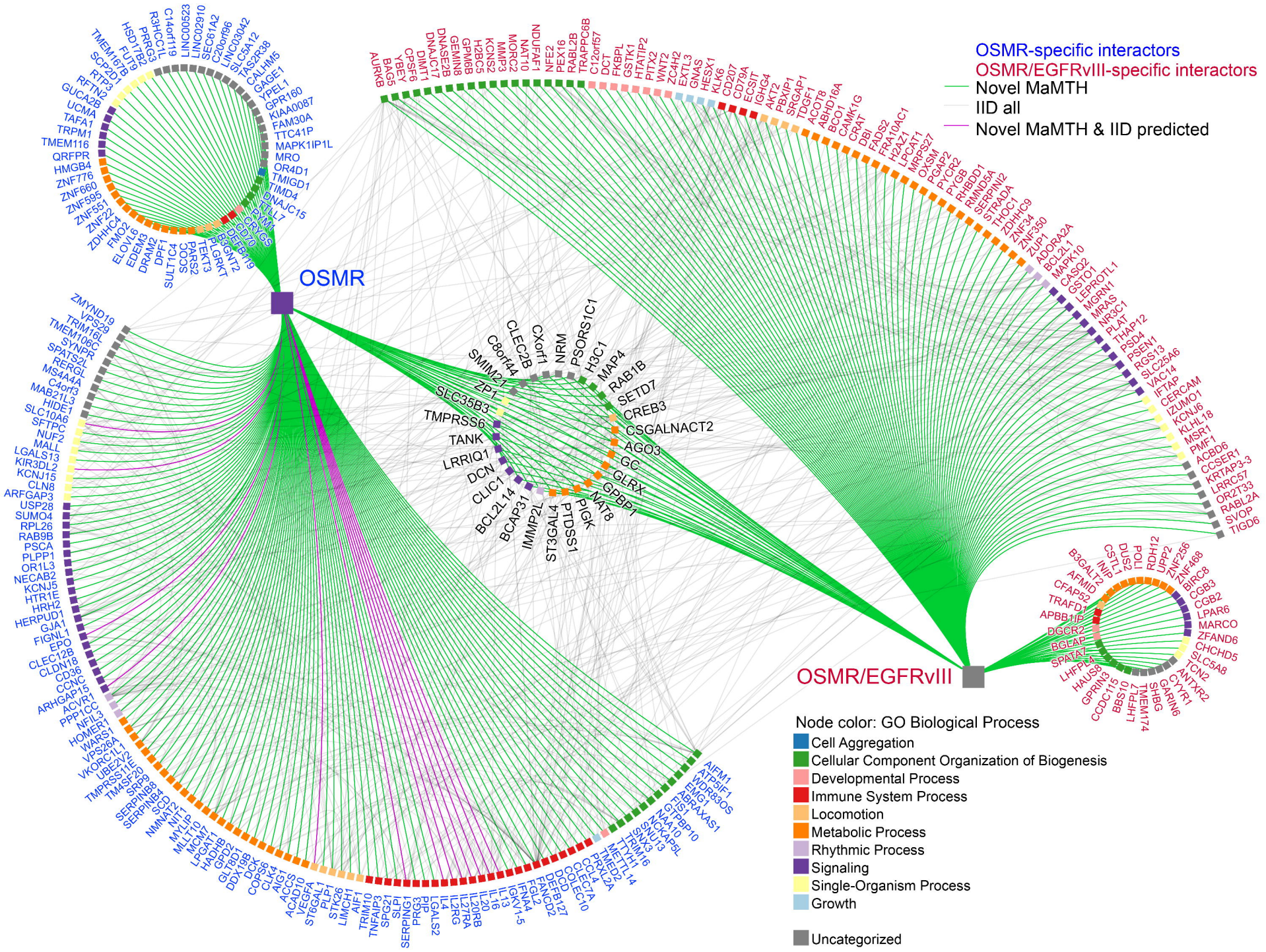
OSMR-specific interactors
OSMR/EGFRvIII-specific interactors
Novel MaMTH
IID all
Novel MaMTH & IID predicted
OSMR
OSMR/EGFRvIII
Node color: GO Biological Process
Cell Aggregation
Cellular Component Organization of Biogenesis
Developmental Process
Immune System Process
Locomotion
Metabolic Process
Rhythmic Process
Signaling
Single-Organism Process
Growth
Uncategorized

Figure 2

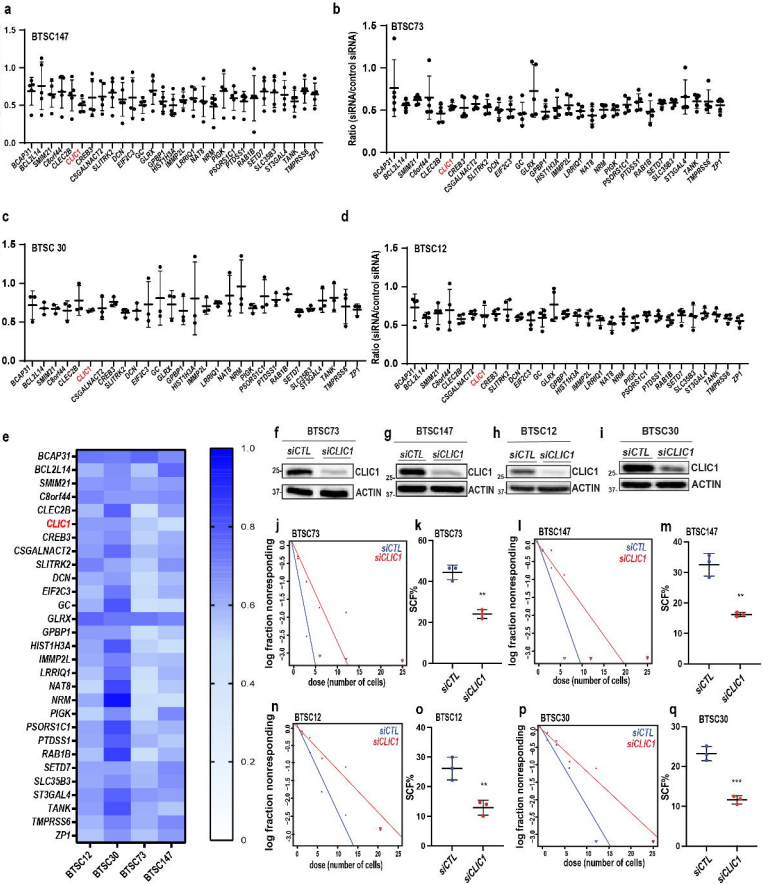
a
BTSC147
b
BTSC73
c
BTSC 30
d
BTSC12
Ratio (siRNA/control siRNA)
BCAP31
BCL2L14
SMMP21
C8orf44
CLEC2B
CLIC1
CREB3
CSGALNACT2
SLITRK2
DCN
EIF2C3
GC
GLRX
GPBP1
HIST1H3A
IMMP2L
LRRIQ1
NAT8
NRM
PIGK
PSORS1C1
PTDSS1
RAB1B
SETD7
SLC35B3
ST3GAL4
TANK
TMPRSS6
ZP1
e
BTSC12
BTSC30
BTSC73
BTSC147
f
BTSC73
g
BTSC147
h
BTSC12
i
BTSC30
siCTL
siCLIC1
CLIC1
ACTIN
j
BTSC73
log fraction nonresponding
dose (number of cells)
k
BTSC73
SCF%
l
BTSC147
m
BTSC147
n
BTSC12
o
BTSC12
p
BTSC30
q
BTSC30

Figure 3

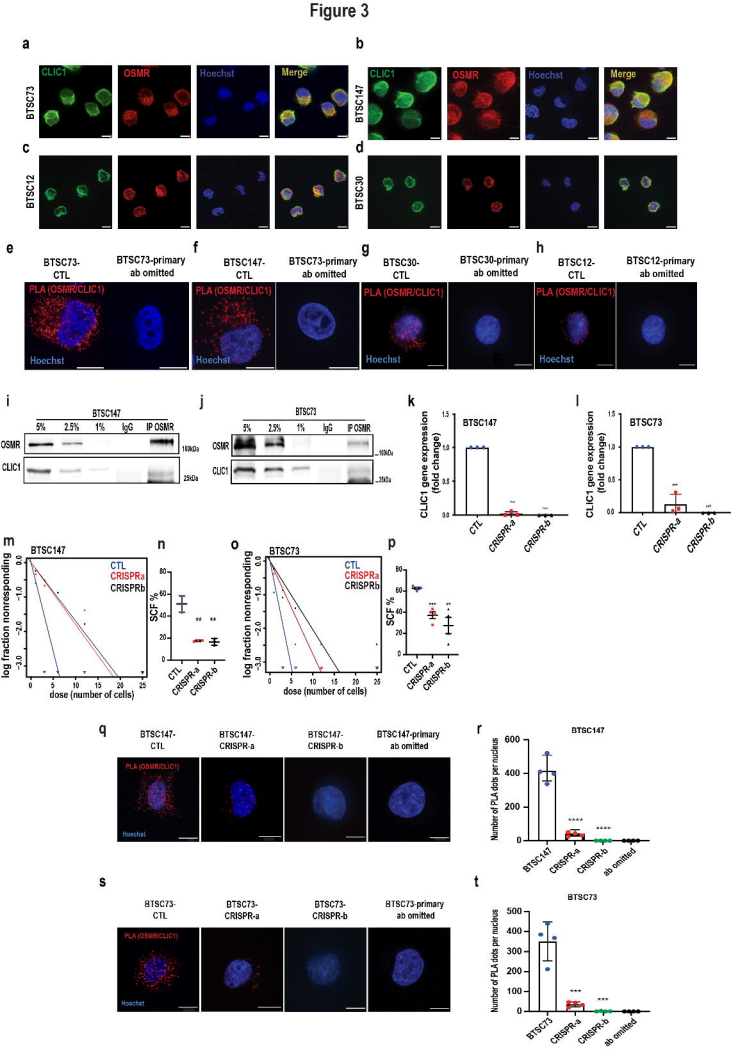
a
CLIC1
OSMR
Hoechst
Merge
BTSC73
b
BTSC147
c
BTSC12
d
BTSC30
e
BTSC73-CTL
BTSC73-primary ab omitted
PLA (OSMR/CLIC1)
Hoechst
f
BTSC147-CTL
g
BTSC30-CTL
BTSC30-primary ab omitted
h
BTSC12-CTL
BTSC12-primary ab omitted
i
BTSC147
5%
2.5%
1%
IgG
IP OSMR
OSMR
CLIC1
110kDa
25kDa
j
BTSC73
k
BTSC147
CLIC1 gene expression (fold change)
CTL
CRISPR-a
CRISPR-b
l
BTSC73
m
BTSC147
CTL
CRISPRa
CRISPRb
log fraction nonresponding
dose (number of cells)
n
SCF %
o
BTSC73
p
q
BTSC147-CTL
BTSC147-CRISPR-a
BTSC147-CRISPR-b
BTSC147-primary ab omitted
r
BTSC147
Number of PLA dots per nucleus
ab omitted
s
BTSC73-CTL
BTSC73-CRISPR-a
BTSC73-CRISPR-b
BTSC73-primary ab omitted
t
BTSC73

Figure 4

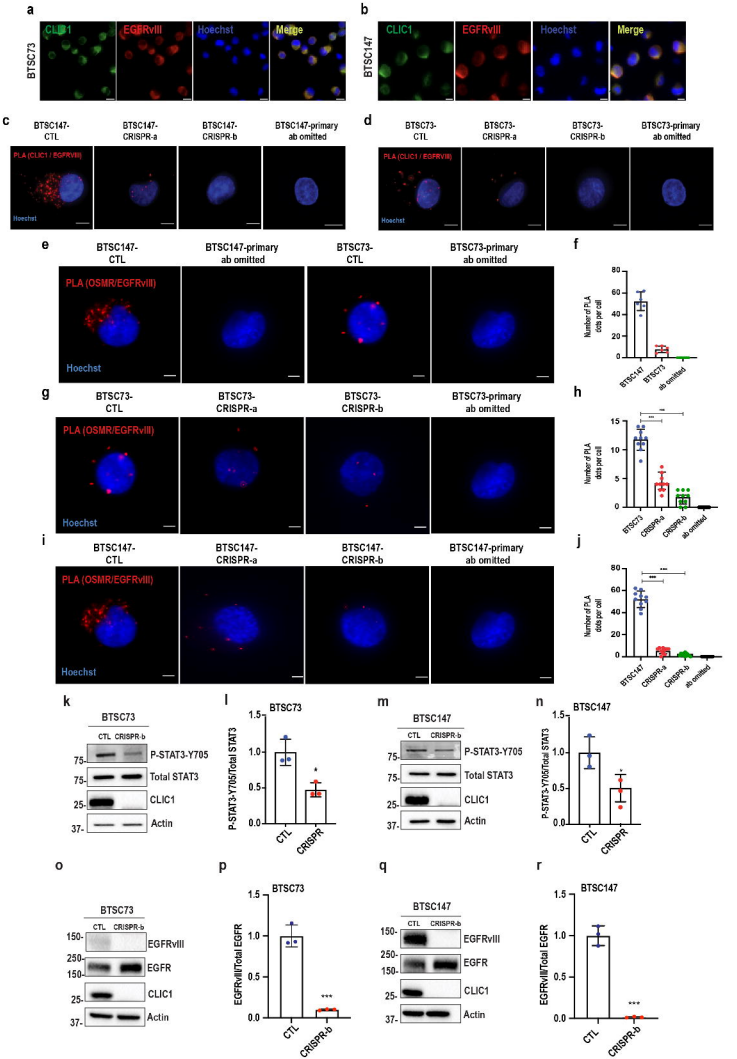
a
BTSC73
CLIC1
EGFRvIII
Hoechst
Merge
b
BTSC147
c
BTSC147-CTL
BTSC147-CRISPR-a
BTSC147-CRISPR-b
BTSC147-primary ab omitted
PLA (CLIC1 / EGFRVIII)
Hoechst
d
BTSC73-CTL
BTSC73-CRISPR-a
BTSC73-CRISPR-b
BTSC73-primary ab omitted
PLA (CLIC1 / EGFRVIII)
Hoechst
e
BTSC147-CTL
BTSC147-primary ab omitted
BTSC73-CTL
BTSC73-primary ab omitted
PLA (OSMR/EGFRvIII)
Hoechst
f
Number of PLA dots per cell
BTSC147
BTSC73
ab omitted
g
BTSC73-CTL
BTSC73-CRISPR-a
BTSC73-CRISPR-b
BTSC73-primary ab omitted
PLA (OSMR/EGFRvIII)
Hoechst
h
Number of PLA dots per cell
BTSC73
CRISPR-a
CRISPR-b
ab omitted
i
BTSC147-CTL
BTSC147-CRISPR-a
BTSC147-CRISPR-b
BTSC147-primary ab omitted
PLA (OSMR/EGFRvIII)
Hoechst
j
Number of PLA dots per cell
BTSC147
CRISPR-a
CRISPR-b
ab omitted
k
BTSC73
CTL
CRISPR-b
P-STAT3-Y705
Total STAT3
CLIC1
Actin
l
BTSC73
P-STAT3-Y705/Total STAT3
CTL
CRISPR
m
BTSC147
CTL
CRISPR-b
P-STAT3-Y705
Total STAT3
CLIC1
Actin
n
BTSC147
P-STAT3-Y705/Total STAT3
CTL
CRISPR
o
BTSC73
CTL
CRISPR-b
EGFRvIII
EGFR
CLIC1
Actin
p
BTSC73
EGFRvIII/Total EGFR
CTL
CRISPR-b
q
BTSC147
CTL
CRISPR-b
EGFRvIII
EGFR
CLIC1
Actin
r
BTSC147
EGFRvIII/Total EGFR
CTL
CRISPR-b

Figure 5

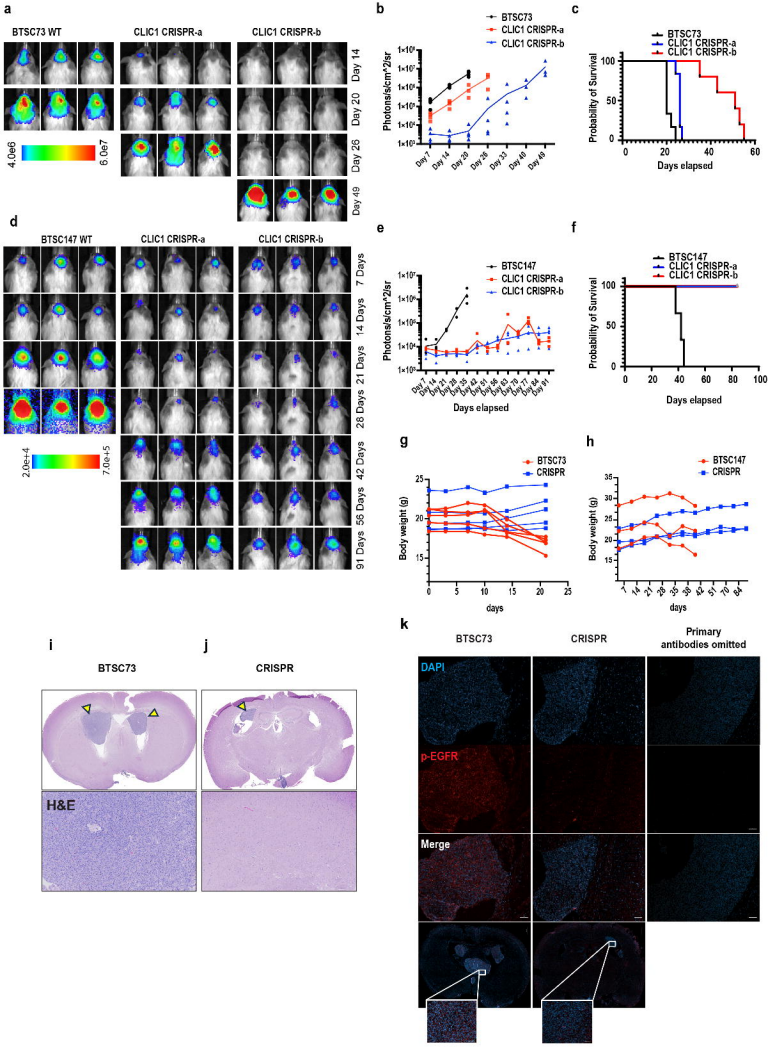
a
BTSC73 WT
CLIC1 CRISPR-a
CLIC1 CRISPR-b
Day 14
Day 20
Day 26
Day 49
4.0e6
6.0e7
b
BTSC73
CLIC1 CRISPR-a
CLIC1 CRISPR-b
Photons/s/cm^2/sr
c
BTSC73
CLIC1 CRISPR-a
CLIC1 CRISPR-b
Probability of Survival
Days elapsed
d
BTSC147 WT
CLIC1 CRISPR-a
CLIC1 CRISPR-b
7 Days
14 Days
21 Days
28 Days
42 Days
56 Days
91 Days
2.0e+4
7.0e+5
e
BTSC147
CLIC1 CRISPR-a
CLIC1 CRISPR-b
Photons/s/cm^2/sr
Days elapsed
f
BTSC147
CLIC1 CRISPR-a
CLIC1 CRISPR-b
Probability of Survival
Days elapsed
g
BTSC73
CRISPR
Body weight (g)
days
h
BTSC147
CRISPR
Body weight (g)
days
i
BTSC73
H&E
j
CRISPR
k
BTSC73
CRISPR
Primary antibodies omitted
DAPI
p-EGFR
Merge

Figure 6

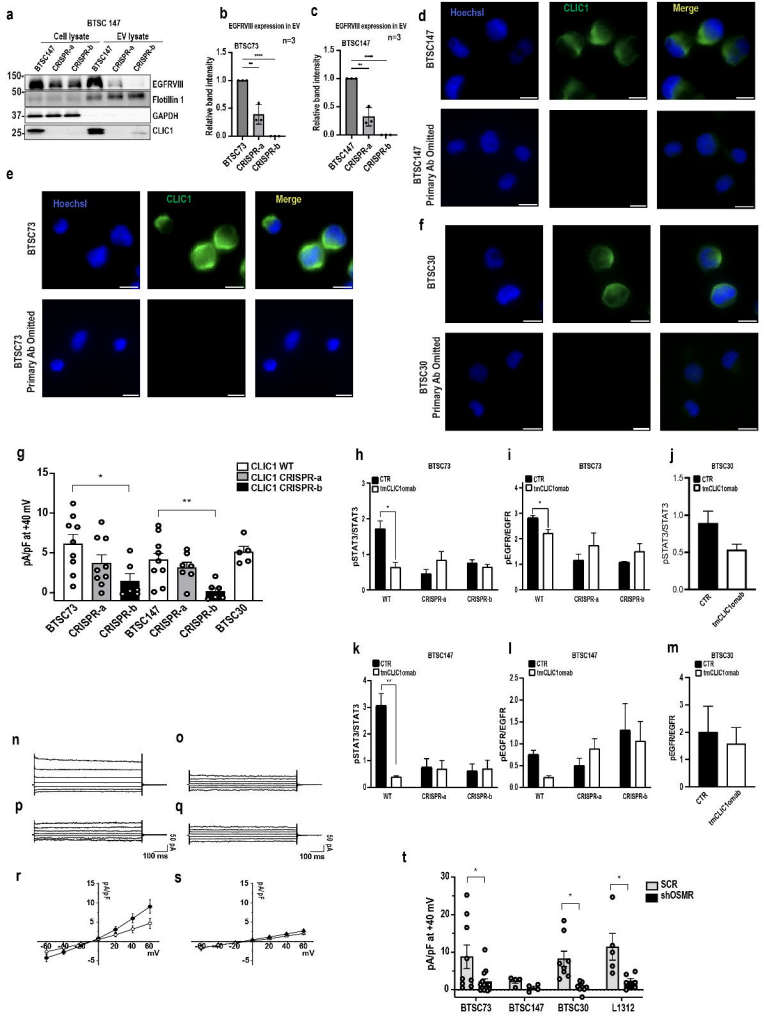
a
BTSC 147
Cell lysate
EV lysate
BTSC147
CRISPR-a
CRISPR-b
150
50
37
25
EGFRVIII
Flotillin 1
GAPDH
CLIC1
b
EGFRVIII expression in EV
BTSC73
n=3
Relative band intensity
c
EGFRVIII expression in EV
BTSC147
n=3
Relative band intensity
d
Hoechst
CLIC1
Merge
BTSC147
BTSC147 Primary Ab Omitted
e
BTSC73
BTSC73 Primary Ab Omitted
f
BTSC30
BTSC30 Primary Ab Omitted
g
CLIC1 WT
CLIC1 CRISPR-a
CLIC1 CRISPR-b
pA/pF at +40 mV
BTSC73
CRISPR-a
CRISPR-b
BTSC147
BTSC30
h
BTSC73
CTR
tmCLIC1omab
pSTAT3/STAT3
WT
i
pEGFR/EGFR
j
BTSC30
k
BTSC147
l
m
n
o
p
q
100 ms
r
s
pA/pF
mV
t
SCR
shOSMR
pA/pF at +40 mV
BTSC73
BTSC147
BTSC30
L1312